TABLE OF CONTENTS MAIN PAGE

TO-98-15-2 (RP-848)

Numerical Simulation of Laboratory Fume Hood Airflow Performance

Allan T. Kirkpatrick, Ph.D., P.E.
Member ASHRAE

Robert Reither

ABSTRACT

A three-dimensional computational fluid dynamics (CFD) analysis has been used to predict airflow patterns in laboratory fume hoods. The simulation includes bypass fume hood primary operational features including the top and bottom bypasses, front airfoils, and rear-slotted baffles. All results were validated experimentally, and the simulation was found to adequately predict fume hood airflow patterns. The results indicate that fume hood flow patterns are highly dependent on inlet flow boundary conditions so that the computation must include the near field room airflow. Additionally, the study included the effects on the fume hood airflow of sash height changes, an operator positioned outside the fume hood, and equipment within the main fume hood chamber. It was shown that for conditions of a fully open sash height, a person in front of the fume hood, and an object inside the fume hood, the fume hood experiences a loss of containment of the flow.

INTRODUCTION

The laboratory fume hood is a safety device used in research, analytical, teaching, and other laboratories. It provides a location at which to work on toxic substances with reduced risk to users. The fume hood basically provides an exhausted enclosure, operating at a negative pressure relative to the room, which vents air away from the user and the laboratory. There are several types of fume hoods including constant volume, variable volume, bypass, restricted bypass, and auxiliary air fume hoods. There are also several styles including bench, distillation, and walk-in, and the fume hoods may have a horizontal sash, vertical sash, or a combination.

This paper discusses the computational modeling of three-dimensional fume hood airflow velocity and patterns. The model in this study simulates a bypass-type bench fume hood with a vertical sash, as shown schematically in Figure 1. Major features of the fume hood are a top-mounted exhaust duct, top bypass supply, fixed bottom bypass under the airfoil, variable-height vertical sash, back baffles, and front airfoils, all of which have been incorporated into this study.

Air enters the main fume hood chamber through one of three locations: sash opening, top bypass, and the bottom bypass formed by the bottom airfoil. The purpose of the top bypass is to maintain a constant volume of air entering the fume hood, regardless of the sash height. A constant-speed fan located above the fume hood exhaust keeps air exiting the fume hood at a constant volumetric rate. The back baffles are positioned such that air is exhausted directly from the work surface as well as the top and center of the main fume hood chamber. The front airfoils reduce the amount of turbulence and eddy motion entering the fume hood. In addition, the bottom airfoil is extended beyond the vertical plain of the sash to provide a direct flow (also called floor sweep) across the bottom of the fume hood main chamber.

At present, fume hoods are designed empirically and tested experimentally. Literature, as reviewed by Pathanjali and Rahman (1996), further indicate that at present only a small number of fume hood studies have been numerical. The study performed by Pathanjali and Rahman (1996) used numerical analysis to study flow patterns inside a simple three-dimensional model of an empty fume hood without back baffles and airfoils. Their study reviewed airflow patterns for different sash heights of fume hoods. Durst and Pereira (1991) performed a numerical analysis of an empty two-dimensional fume hood model, which included a back baffle, to support their experimental results. Durst and Pereira studied containment capabilities of fume hoods at selected sash openings. Chang (1994) experimentally studied the velocity profiles around manikins placed in front of the fume hood. Inclusion

Allan T. Kirkpatrick is a professor and **Robert Reither** is a graduate student at Colorado State University, Fort Collins.

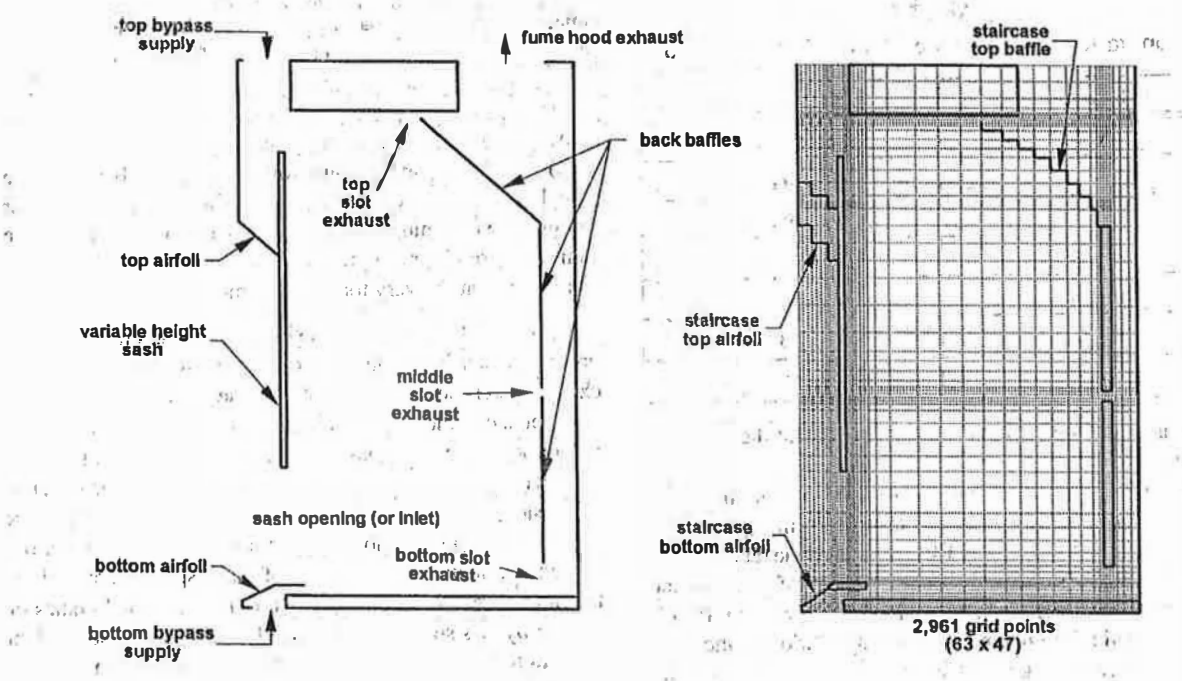

Figure 1 *Fume hood features and associated computational grid.*

of the airfoils, bypasses, and angled slotted baffles in this study furthers the previous numerical studies (Pathanjali and Rahman 1996; Durst and Pereira 1991) performed on fume hoods. The inclusion of the person and object in the fume hood chamber provides a numerical study comparison to Chang's (1994) experimental work.

COMPUTATIONAL MODEL

A turbulent finite difference model was used for the simulation (Kurabuchi et al. 1989). The computational model uses a standard two-equation k-ε model with buoyancy terms included. The k-ε model was selected because it is relatively stable and computationally efficient compared with the more complicated Reynolds stress models and is applicable to a wide range of turbulent flows (Neilsen 1998). There are seven nondimensional equations used by the model: two vector partial differential equations (continuity, momentum), two scalar differential equations (turbulence kinetic energy, dissipation rate of turbulence energy), and one algebraic relationship for turbulent viscosity.

Continuity:

$$\frac{\partial u_j}{\partial x_j} = 0$$

Momentum:

$$\frac{\partial u_i}{\partial t} + u_j\frac{\partial u_i}{\partial x_j} = -\frac{\partial(p+2\rho k/3)}{\rho\partial x_i} + \frac{\partial}{\partial x_i}\left\{(\nu+\nu_t)\left[\frac{\partial u_i}{\partial x_j}+\frac{\partial u_j}{\partial x_i}\right]\right\} - \beta g_i\theta$$

Turbulent Kinetic Energy:

$$\frac{\partial k}{\partial t} + u_j\frac{\partial k}{\partial x_j} = \frac{\partial}{\partial x_j}\left[\frac{\partial k}{\partial x_j}\left(\nu+\frac{\nu_t}{\sigma_k}\right)\right] + \nu_t\left(\frac{\partial u_i}{\partial x_j}+\frac{\partial u_j}{\partial x_i}\right)\frac{\partial u_i}{\partial x_j} + \beta g_i\frac{\nu_t}{\sigma_\theta}\frac{\partial\theta}{\partial x_i} - \varepsilon$$

Dissipation Rate of Turbulence Energy:

$$\frac{\partial \varepsilon}{\partial t} + u_j\frac{\partial \varepsilon}{\partial x_j} = \frac{\partial}{\partial x_j}\left[\frac{\partial \varepsilon}{\partial x_j}\left(\nu+\frac{\nu_t}{\sigma_\varepsilon}\right)\right] + \frac{\varepsilon}{k}\left[C_1\nu_t\frac{\partial u_i}{\partial x_j}\left(\frac{\partial u_i}{\partial x_j}+\frac{\partial u_j}{\partial x_i}\right)\right] - C_2\varepsilon + C_3\beta g_i\frac{\nu_t}{\sigma_\varepsilon}\frac{\partial\theta}{\partial x_i}$$

Turbulent Viscosity:

$$\nu_t = C_D\frac{k^2}{\varepsilon}$$

There are also seven required empirical constants determined from correlations of experimental data (Launder and Spalding 1974). The constants are shown in Table 1.

To solve the system of nonlinear partial-differential equations, the code uses an explicit time marching algorithm, pressure relaxation method, and a central or upwind differencing scheme (Kurabuchi et al. 1989). A marker and cell method is used for the staggered grid. Velocity components are defined at the center of their normal cell faces and the scalar variables (pressure, temperature, turbulence kinetic energy, and dissi-

TABLE 1
κ-ε Constants for Use in the Fume Hood Simulation

κ-ε Constant	Value
C_D	0.09
C_1	1.44
C_2	1.92
C_3	1.0
σ_k	1.0
σ_ε	1.3
σ_θ	0.9

pation rate of turbulence energy) are defined at the center of the cell.

The wall boundary condition for the momentum boundary layer used by the code is based upon the power law assumption of the velocity profile. In general, the real cell next to the wall is assumed to lie in the power law profile region and the dummy cell in the wall is set to a constant fraction (0.714) of the real cell at the beginning of each iteration. k and ε are assumed to have zero gradient at the wall. A detailed description of these boundary conditions can be found in Knapmiller and Kirkpatrick (1994).

On two of the fume hood configurations to be discussed later, a contaminant dispersion study was performed using a turbulent contamination diffusion model (Kurabuchi et al. 1989). The converged flow field output file from the flow field calculation is used as input for computing the contaminant dispersion since the velocity field is independent of the concentration field. The following equation for the conservation of contaminant species is solved:

$$\frac{\partial c}{\partial t} + \frac{\partial c u_j}{\partial x_j} = \frac{\partial}{\partial x_j}\left[\left(D + \frac{\nu_t}{\sigma_c}\right)\frac{\partial c}{\partial x_j}\right] + s$$

TWO-DIMENSIONAL COMPUTATIONAL DOMAIN AND INLET BOUNDARY CONDITIONS

In a laboratory fume hood, one of the major flow structures in the fume hood is the large vortex behind (downstream of) the sash (Sanders 1993). An acceptable CFD model of a fume hood should be able to approximate the size, shape, and direction of this large vortex at a minimum. In order to achieve this, appropriate boundary conditions must be applied to the fume hood simulation. It should be emphasized that at present, an acceptable CFD fume hood model is limited by the fact that it calculates a time-averaged solution at a point in time that is static. The airflow inside a fume hood is turbulent and unsteady in nature and as such cannot be fully characterized by any CFD models at this time.

A two-dimensional version of the fume hood simulation was used to investigate the required boundary conditions for flow entering the fume hood. The grid (63 - x direction, 47 - y direction) used is shown in Figure 1. The grid contains objects (impenetrable barriers as seen by the fume hood simulation) to represent the structure of the fume hood: sash, top and bottom front airfoils, lower, middle, and top back baffles. In the model, as in the actual fume hood, flow can enter the fume hood in one of three ways: the main inlet (in front of the sash), top bypass supply, and bottom bypass. Also, as in the actual fume hood, flow can exit the main fume hood chamber through the top, middle, or bottom slot exhausts and exits the fume hood only through the rectangular exhaust (upper right of Figure 1) at the very top of the fume hood.

To validate the two-dimensional computational work and provide actual inlet boundary conditions to the calculations, experimental measurements of the inlet and exit flows were made on a commercially available laboratory fume hood. The laboratory fume hood has a vertical sash with an air bypass system to maintain a relatively constant exhaust velocity. It has dimensions of approximately 54 in. × 72 in. × 36 in. (1.37 m × 1.83 m × 0.91 m), without the cabinet (or bench) it is set on. The experimental measurements of the airspeed were made at the three fume hood air entrances in the horizontal planes of the top bypass supply and bottom bypass and in the vertical plane of the sash in the fume hood sash opening. Each entrance was divided into equal rectangular grids, and measurements were taken at the center of each grid and averaged over time in concurrence with *ANSI/ASHRAE Standard 110* (1995). For each entrance, the measurements at each grid point were averaged together to find an average airspeed for that entrance at a selected sash height. As an example, experimental average face velocity measurements for the fume hood sash opening are listed in Table 2. These average airspeeds were used as input to the initial two-dimensional fume hood simulations.

TABLE 2
Experimental Face Velocity Measurements at Selected Sash Heights

Sash Height in.	Experimental Face Velocity fpm
5.5	266
11	206
18 (Working Height)	156
22	130
30.25 (Fully Open)	95

The simplest inlet boundary conditions for the fume hood simulation are one of uniform flow at the three entrances (top bypass, bottom bypass, and sash opening) to the fume hood. At each entrance, the experimentally measured airspeed was input as a uniform flow to the fume hood simulation. The results of this boundary condition are shown in Figure 2. For these boundary conditions, a large counterclockwise vortex is formed near the back baffles and a smaller clockwise vortex is formed behind (downstream of) the top of the sash. This flow

BACK TO PAGE ONE

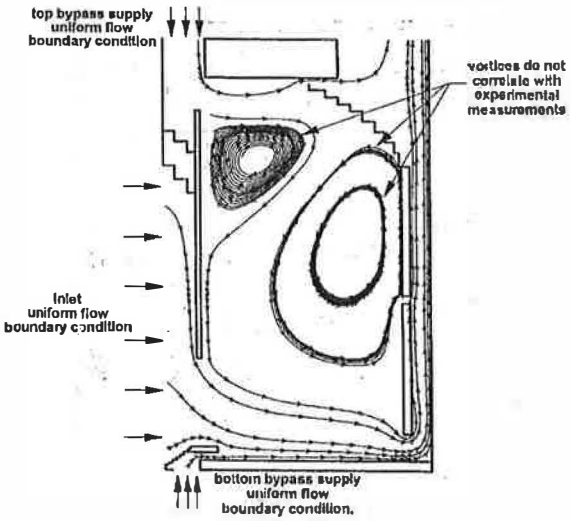

Figure 2 *Uniform flow boundary conditions.*

structure contradicts the expected pattern from the experimental results, which is a large vortex starting at the bottom of the sash rotating counterclockwise.

As can be seen in Figure 2, flow entering the top of the fume hood inlet is quickly turned downward towards the sash opening. This causes the air entering at the top of the sash opening to have a downward angle to it. Smoke tests performed on an actual fume hood showed flow entering horizontally throughout the sash opening. This in addition to the out-of-place-and-size vortices leads to the conclusion that the uniform flow boundary condition produces incorrect results.

The computation shows it is necessary to have the actual inlet velocities, at the appropriate angles, as boundary conditions to the fume hood model. To accomplish this, a room approximately 8 ft high by two fume hood depths (~ 58 in., 1.48 m) was added to the fume hood model. The u and v velocities were then extracted from a completed computation of the room and fume hood flow at the grids just outside the fume hood sash opening, top bypass, and bottom bypass. These velocities at each of the three entrances were then used as boundary conditions to the fume hood model.

The results are shown in Figure 3. It is emphasized that the grids used for the simulations in Figures 2 and 3 are exactly the same. The input files are also exactly the same except for the flow boundary conditions at the inlet, top bypass, and bottom bypass. Now, at each of the entrances, u and v velocities are applied. As desired, there is a large counterclockwise vortex at the bottom of the sash. In addition, there is only a slight downward angle to flow entering the sash opening at the top and the flow appears to enter horizontally for the most part throughout the sash opening. It should be noted that this vectored input was applied to the top and bottom bypasses as well as the inlet.

Figure 4 shows the flow structure predicted by the computation including the room and fume hood. In this model, a uniform flow boundary condition is applied at the room

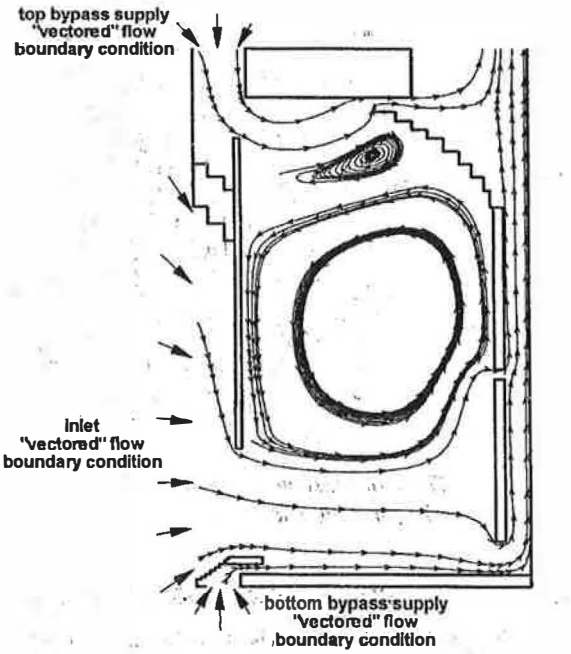

Figure 3 *Vectored flow boundary conditions.*

entrance. The magnitude of the velocity required is obtained with a mass balance. The velocity of the airflow entering the room was calculated by adding the mass flow rates at the inlet, bottom bypass, and top bypass, and dividing by the room frontal area. Velocities at the fume hood entrances are an output from the fume hood simulation. As expected, the flow structure inside the fume hood is the same as that given by the fume hood model with vectored input.

Thus, the two-dimensional computations show that a room and bypass fume hood should be modeled together, with the uniform velocity input at the far field of the room, not at the fume hood entrances.

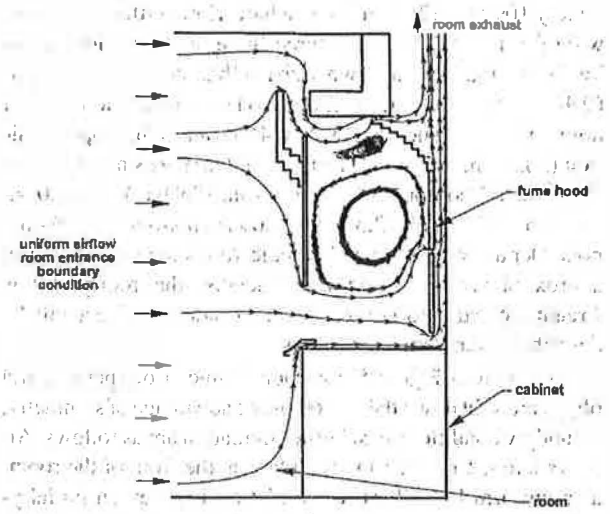

Figure 4 *Room and fume hood airflow patterns.*

BACK TO PAGE ONE

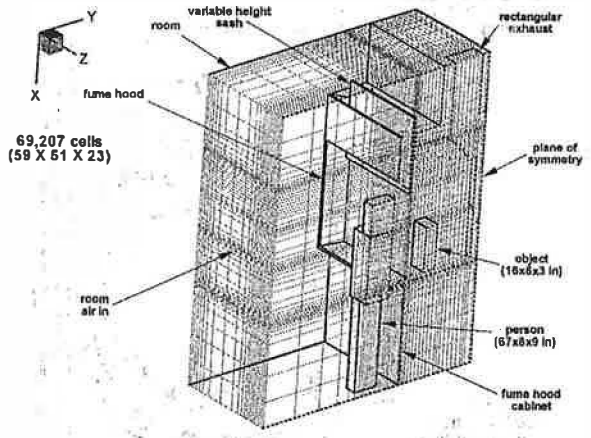

Figure 5 *Three-dimensional room and fume hood configuration and grid.*

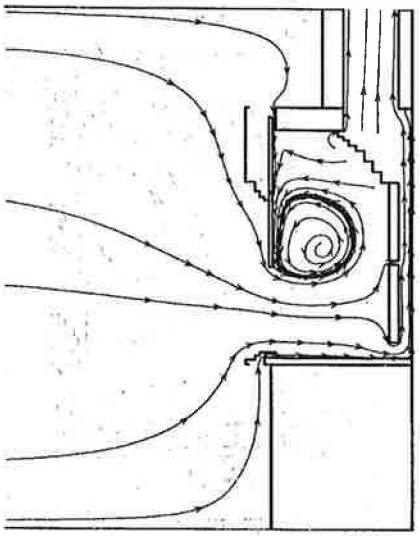

Figure 6 *Working sash height (18 in., 0.46 m) airflow pattern, computational results.*

THREE-DIMENSIONAL COMPUTATIONAL MODEL

The airflow in a fume hood is three-dimensional due to the finite width of the main chamber, the airfoils, and the presence of a person and object in front of and inside the fume hood, respectively. The three-dimensional computational grid used to model the room and the laboratory fume hood is shown in Figure 5. The model has a room containing the fume hood resting on a cabinet, a rectilinear person standing on the floor in front of the fume hood, and an object inside the fume hood. In addition, the model contains a variable height sash, top, bottom, and side airfoils; top, middle, and bottom baffles; and a rectangular exhaust. The rectangular exhaust approximates the round collar in the actual fume hood. The fume hood dimensionally is as close as possible to an actual laboratory fume hood. The person and object size are as specified in *ANSI/ASHRAE Standard 110* (1995). The room is approximately 109.5 in. (2.78 m) high, a half width of the fume hood wide (36 in., 0.91 m), and three fume hood interior depths long (83.5 in., 2.12 m). Two sash heights were studied, 18 in. (0.46 m) and 30.25 in. (0.77 m). These were selected as a nominal working height (18 in., 0.46 m) and a fully open position (30.25 in., 0.77 m). The three slot exhausts heights were fixed for all computations at 0.75 in. (0.01 m) top, 1.0 in. (0.03 m) middle, and 3.375 in. (0.09 m) bottom. Three fume hood depths were selected for the room length because at approximately 2.5 fume hood depths, the room airflow streamlines start to curve. Figures 6 and 9, which will be described later, demonstrate this.

As seen in Figure 5, the room, fume hood, person, and object are split down the center to take advantage of symmetry. Boundary conditions to start the simulation are as follows. Air flows into the room, on the *xz* plane at the front of the room, as a uniform flow. This room inlet air is given an initial *y*-velocity, turbulence energy, and a turbulence dissipation rate. The nondimensional turbulence energy of the room inlet air is 0.005, and the nondimensional turbulence dissipation rate is 0.00125; both values are typical of room air motion computations (Kurabuchi et al. 1989). The nondimensional turbulence energy corresponds to a turbulent intensity of 5.8%. The room exhaust is through the rectangular exhaust at the top of the fume hood, where only the pressure is specified and the velocity is computed by the model. Power-law wall boundary conditions are specified on the ceiling and floor of the room as well as on the back surface of the fume hood. All other surfaces, including those of the fume hood, the person, and the object, have a zero normal velocity boundary condition with no shear.

Grid development of a fume hood model proved to be a very challenging problem. The actual fume hood contains three very thin airfoils, all at different angles, as well as a very thin top baffle at yet another angle. All these angled surfaces are modeled as staircases with an infinitely thin surface between adjacent cells, which have zero normal velocity. There are also three differently sized flow entrances, each having their own direction, and four exhausts of different sizes in two different directions. The grid contains 69,207 nonuniform cells (59 - *x* direction, 51 - *y* direction, 23 - *z* direction) optimized by size, location, and number of cells to include all of the above features, as well as the person, object, and variable height sash in the same grid. This allowed configuration changes by changing boundary conditions without having to perform a time consuming grid restructuring process. The nominal computation time is 22 hours on a 200 MHz Pentium Pro desktop PC.

A grid sensitivity study was performed on a two-dimensional model of the room and fume hood in Figure 5. The *x*-*y* plane of symmetry was used as the two-dimensional computational domain. A two-dimensional sensitivity study was

used for simplicity and reduced computation time since the aforementioned two-dimensional results in the previous section agreed well with the experiment. The baseline grid of cells with 59-x direction and 51-y direction was compared with a grid of double the size (all cells were split in half) with 115-x direction and 99-y direction. In each coordinate direction, the grid contains three dummy cells that were not split in half. Streamline plots and mass balances were compared for each grid. The streamline plots were almost identical and differences were only discernable by superimposing the two plots. The mass balances were identical for the three incoming flows (sash opening, top bypass, bottom bypass), and there was only a 1% difference in the slot exhaust flows (top, middle, and bottom). With these small changes, the baseline grid was deemed adequate for the computations.

The convergence of the model was judged by tracking the volumetric root mean square of the residual of the momentum equation. A solution was considered to be converged if the first two significant figures of volumetric root mean square momentum residual did not change for approximately 100 iterations (Kurabachi et al. 1990). This occurred in the 26,000 to 29,000 iterations range for most of the computations performed. As an example, the value of the volumetric root mean square momentum residual was 0.00028 for the empty room and fume hood set at the working height (18 in., 0.46 m).

EMPTY FUME HOOD COMPUTATION AND MODEL VALIDATION

To validate the computations at each sash height, a smoke test and a mass balance were performed on an empty fume hood. As described earlier in the inlet air boundary condition studies, airflow velocities were measured at selected points in concurrence with *ANSI/ASHRAE Standard 110* (1995), in the sash opening, top bypass, bottom bypass, top slot exhaust, middle slot exhaust, and bottom slot exhaust. These measured velocities were averaged to find an average velocity for each of the six flow channels. The mass flow is then calculated from the product of the average velocity and its associated area for each of the aforementioned six flow channels.

In Figure 6, the computational results of the 18 in. (0.46 m) sash height are shown. Figure 6 represents a vertical slice through the room and fume hood taken at the plane of symmetry. As can be seen, the flow enters the room from the left and enters the fume hood at any of the three entrances: sash opening, top bypass, or bottom bypass. The flow then exits the main fume hood chamber through the top, middle, or bottom slot exhausts. Flow exits the room through the exhaust at the top of the fume hood. As mentioned above, the main flow structure expected is a large counterclockwise vortex behind (downstream of) the bottom of the sash, which the computation is able to produce.

Figure 7 shows the smoke test for the 18 in. (0.46 m) sash height. All smoke test results are hand-drawn two-dimensional representations of what was viewed in the fume hood. It should be noted that these smoke test results show the time averaged flow patterns. The smoke traces exhibited unsteady characteristics during the tests. As predicted by the simulation, there is a large counterclockwise vortex behind (downstream of) the bottom of the sash. The only discrepancy is that the vortex in Figure 7 smoothly follows the back baffles almost to the top of the top baffle in the fume hood main chamber, where as the vortex in Figure 6 breaks off at the middle of the top baffle in the fume hood main chamber. This is most likely due to the top baffle being represented by a staircase instead of smooth angled surface.

A mass balance comparison for the 18 in. (0.46 m) sash height is shown in Table 3. For each flow channel, the volume

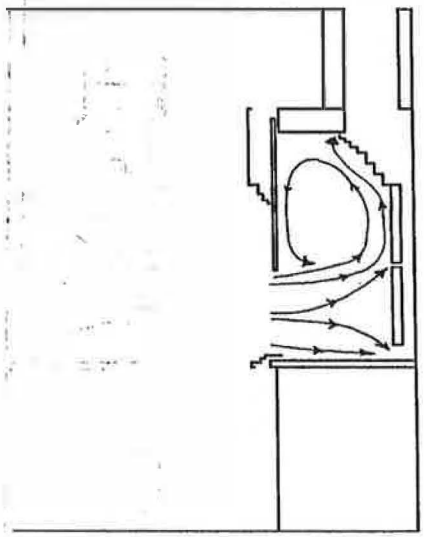

Figure 7 Working sash height (18 in., 0.46 m) airflow pattern, smoke test results.

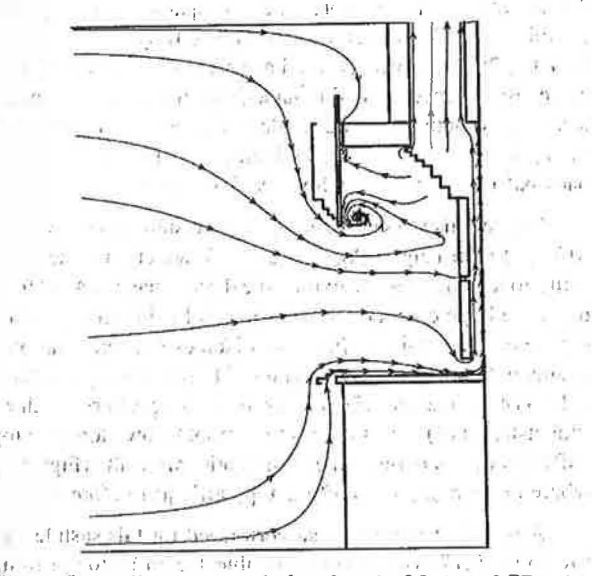

Figure 8 Fully open sash height (30.25 in., 0.77 m) airflow pattern, computational results.

TABLE 3
18 in. (Working Height) Sash Height Mass Balance

	Flow Channel	Experimental Flow %	Computational Flow %
Inlet Flow	Inlet	90	92
	Top Bypass	4	4
	Bottom Bypass	6	4
Exhaust Flow	Top Exhaust	23	24
	Middle Exhaust	29	17
	Bottom Exhaust	48	59

TABLE 4
30.25 in. (Fully Open) Sash Height Mass Balance

	Flow Channel	Experimental Flow %	Computational Flow %
Inlet Flow	Inlet	93	95
	Top Bypass	2	2
	Bottom Bypass	5	3
Exhaust Flow	Top Exhaust	24	25
	Middle Exhaust	28	19
	Bottom Exhaust	48	56

flow percentage is compared experimentally and computationally. As shown in Table 3, the fume hood entrances compare very well with the experimental values (within 3%). At the exhausts, the top slot exhaust compares favorably while the middle and bottom slot exhausts are off by approximately 11% to 12%. This was deemed as acceptable based upon the close resemblance of the simulated flow structure to the smoke test flow structure. Future model changes may be made to improve the performance, including adding friction to the back baffles and the fume hood cabinet surfaces.

Figure 8 displays the computational results for the 30.25 in. (0.77 m) sash height. Again we see flow entering the three fume hood entrances and exiting the three exhausts. As before, there is a large counterclockwise vortex behind (downstream of) the bottom of the sash. Comparison of the computational results with the smoke test results of Figure 9 is again favorable. The smoke test (Figure 9) shows a larger vortex behind (downstream of) the sash with the smooth flow along the top baffle, in comparison to the computational results (Figure 8) where the vortex breaks off the top baffle just before the top.

A mass balance was also performed for this sash height (30.25 in., 0.77 m), as shown in Table 4. Similar to the 18 in. (0.46 m) sash height mass balance, there are favorable comparisons at the three entrances and the top slot exhaust. The model again deviates from experiment at the middle and bottom slot exhausts (by approximately 8% to 11%).

These two sash height computations, when compared to accompanying smoke tests and mass balances, indicate that the main features of the actual three-dimensional fume hood airflow can be replicated with CFD analysis.

EFFECTS OF A PERSON AND OBJECT ON FUME HOOD PERFORMANCE

As shown in Figure 5, the model was configured to be more realistic by including a person standing in front of the fume hood and an object inside the fume hood. With these additions to the model, the same two sash height cases were studied, working height (18 in., 0.46 m) and fully open (30.25 in., 0.77 m). For model validation purposes, smoke tests were performed on both test cases. No mass balance was performed.

Figures 10 and 11 display the computational results for the case of the sash height set at 18 in. (0.46 m), a person in front of the fume hood, and an object placed in the main fume hood chamber at a distance of 6 in. (0.15 m) behind the sash and 1.5 in. (0.04 m) above the cabinet. Figure 10 and subsequent similar figures show a vertical plane cut at the plane of symmetry of the model. This vertical plane cuts through the space between the person's legs indicating the flow passes between the person's legs and up into the fume hood. The dashed lines below the person represent the location of the person's legs in another vertical plane and are there for reference only. Figure 11 and subsequent similar figures represent a horizontal slice through the room and fume hood. The horizontal slice is located such that for a fully open sash (30.25 in.), the horizontal plane is at the center height of the sash opening. This location is approximately chest level on the person and

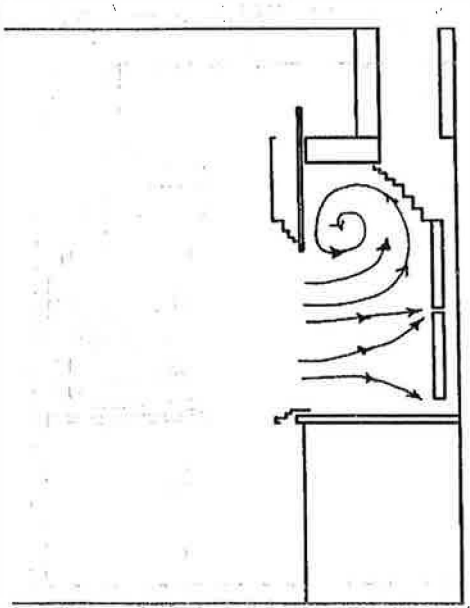

Figure 9 Fully open sash height (30.25 in., 0.77 m) airflow pattern, smoke test results.

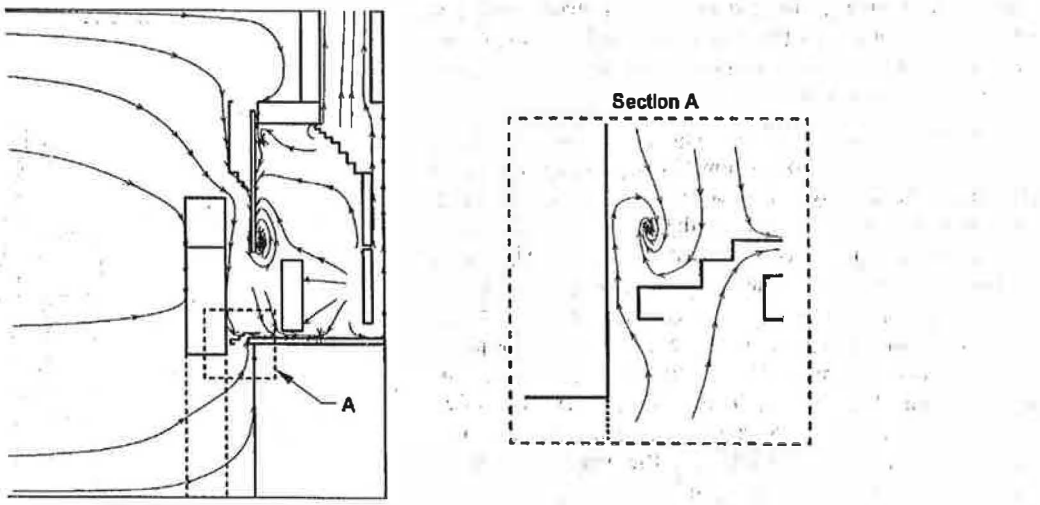

Figure 10 Working sash height (18 in., 0.46 m), vertical slice, person, object at 6 in. (0.15 m), computational results.

one-third the way down from the top of the object. Other than the inclusion of the person and object in this model, the computational grid and inlet boundary conditions are identical to the aforementioned models.

As shown in Figure 10, a vortex appears behind (downstream of) the sash, although smaller in size compared to the empty room and fume hood of Figure 6. Additionally, adding a person to the model generates a small clockwise vortex behind (downstream of) the person at approximately waist level. Details of this small vortex are shown in Section A of Figure 10. The vortex is generated by flow over the top of the person and down its body, as well as the flow coming up between the person's legs and moving up its body. The other interesting flow pattern is on top of and directly behind (downstream of) the object. The airflow does not shoot over the top, but instead flows backward from the bottom baffle towards the object. Directly behind (downstream of) the object, approximately one third of the flow goes up and mixes into the vortex behind (downstream of) the sash and the remaining two-thirds moves down the object and exits through the bottom slot exhaust. Lastly, even with the person and object in the model, the computation predicts that containment is maintained by the fume hood, i.e., there is no reverse flow out of the fume hood entrance.

Of interest in the horizontal slice of Figure 11 is a small vortex appearing downstream in the lee of the person and a large vortex appearing just downstream of the object. The vortex just downstream of the person is generated from the flow around the sides of the person. With the sash down at 18 in. (0.46 m), most of the flow entering the hood is forced past the

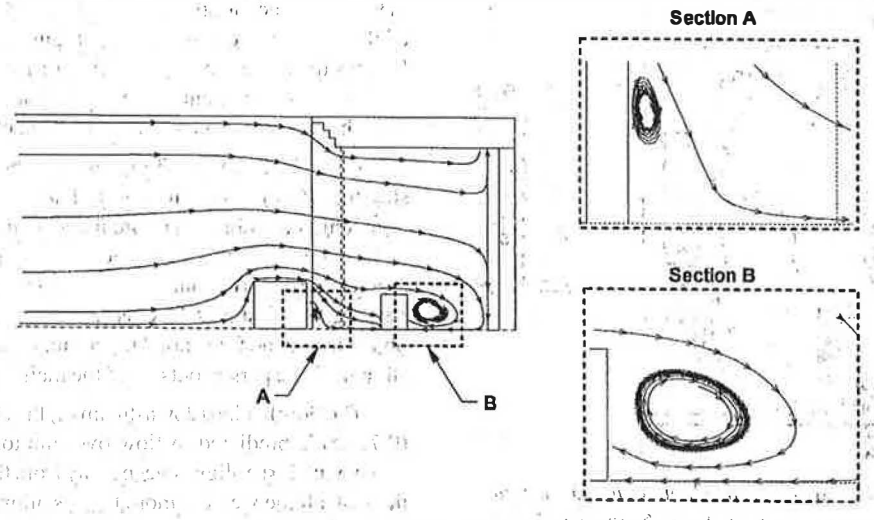

Figure 11 Working sash height (18 in., 0.46 m), horizontal slice, person, object at 6 in. (0.15 m), computational results.

object and as such a strong vortex is generated just downstream of the object. Again, it should be noted that all of these descriptions are two-dimensional projections of a three-dimensional flow structure.

A nondimensional pressure contour plot of a vertical slice of the room and fume hood is shown in Figure 12. The vertical plane is the plane of symmetry, as in Figure 10. The pressure contour details the area of interest, the main fume hood chamber, and the room just outside the sash. The pressure is nondimensionalized by the dynamic pressure, with the average sash velocity used as the scaling velocity. The pressure contour confirms the streamline plot of Figure 10. There is a low pressure behind (downstream of) the sash where the large vortex is, and there is a high pressure in front of the lower back baffle, which pushes the airflow towards the object. A low pressure region also exists behind the back baffle, where the flow is drawn up and out of the fume hood.

The smoke test results of this configuration are shown in Figure 13, where again it should be noted that smoke test results show the time-averaged flow structure and not some of the unsteady characteristics the actual flow exhibits. No horizontal drawings of the smoke tests were recorded and, as such, only the vertical slices are described. Comparisons between the smoke test and the computation show the computation accurately predicts the size and location of the small vortex behind (downstream of) the person, the general flow structure behind (downstream of) the object, and containment of the flow inside the main fume hood chamber. The computation does not exactly match the smoke test results in its prediction of the flow over top of the object and the size of the vortex behind (downstream of) the sash. No explanation has been found for the discrepancy in the flow over the top of the object, but the vortex size is most likely attributed to the staircase

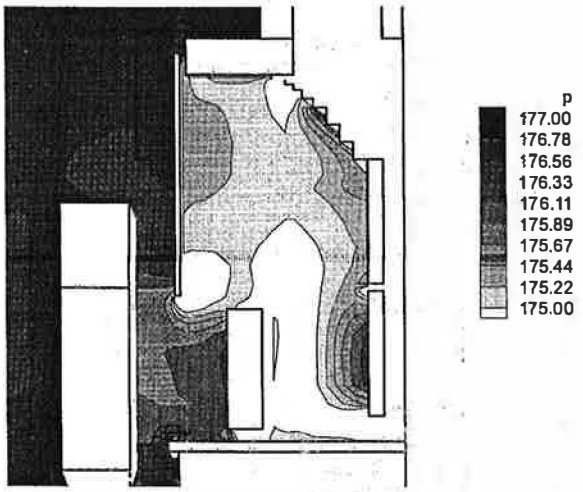

Figure 12 *Working sash height (18 in., 0.46 m), vertical slice, person, object at 6 in. (0.15 m), nondimensional pressure contour.*

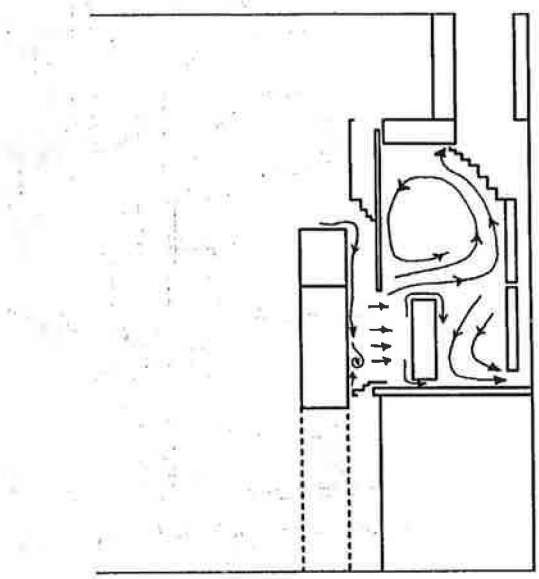

Figure 13 *Working sash height (18 in., 0.46 m), vertical slice, person, object at 6 in. (0.15 m), smoke test results.*

baffle, as mentioned before. Additionally, no vortices are seen in the head area of the person and the flow goes over the top of the head, down the face, and continues at the body. Chang (1994) reported that, in general, the airflow seemed to flow over the head and down the body for similar fume hood and sash-height configurations. Chang also reported infrequent vortices in the facial area, which are representative of the unstable characteristics of the flow.

A contamination study was performed on the working height (18 in., 0.46 m) configuration. A concentration of the contaminant, nondimensionally, set to 1.0 is applied to the top of the object. All other surfaces in the model have a nondimensional concentration of 0.0. Figure 14 displays the results of this computation. As seen in Figure 14, the contaminant follows the airflow patterns in Figure 10. A small concentration of the contaminant moves to the back of the sash, but the fume hood still maintains the containment.

In the 30.25 in. (0.77 m) sash-height study, similar flow structures (vortices behind the sash and person and recirculation behind the object) are predicted as in the 18 in. (0.46 m) sash-height case. However, the most significant result is the prediction of loss of containment in the main fume hood chamber. Figure 15 shows flow is moving from the front of the object inside the fume hood to the small vortex behind (downstream of) the person outside of the main fume hood chamber.

The flow behind (downstream of) the object in the 30.25 in. (0.77 m) is predicted to flow over the top of the object and down, with just a slight sweep away from the back baffle. With the sash all the way up, more flow is allowed to pass over the top of the object and less flow is forced around the sides, as seen before in the 18 in. (0.46 m) sash-height case. Section A

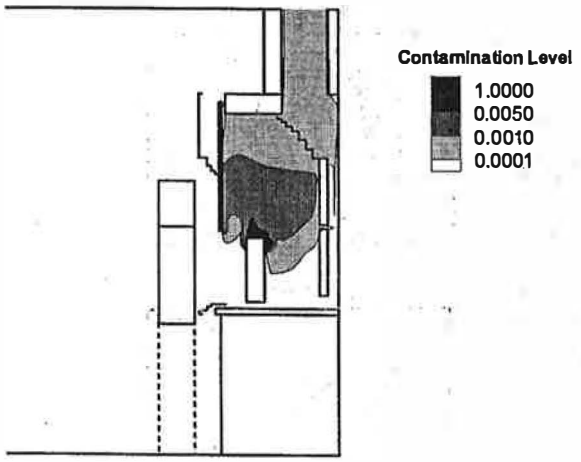

Figure 14 *Working sash height (18 in., 0.46 m), vertical slice, person, object at 6 in. (0.15 m), nondimensional contamination results.*

of Figure 15 shows a small clockwise vortex behind (downstream of) the person of the same size as before but located a little higher above the waist. Figure 16 represents the horizontal slice for this configuration. A strong vortex now appears just downstream of the person and a weak flow recirculation exists just downstream of the object. For the fully open sash height, flow is no longer forced down the body of the person by the sash; consequently, the flow around the sides of the person generates a vortex. Since the flow is not as strong around the object, a weak airflow recirculation appears behind (downstream of) the object, also in contrast to the 18 in. (0.46 m) sash height.

Figure 17 displays the nondimensional pressure contour for this configuration. There is a high pressure region just in front of the top of the object and a low pressure region in front of the object extending out beyond the plane of the sash. As shown in the streamline plot of Figure 15, the pressure contour also shows airflow will travel from the top of the object towards the bottom and out of the fume hood. Also shown is a high pressure at the lower back baffle allowing airflow to move towards the back of the object. In comparison to the working height pressure contour of Figure 12, the pressure difference between the front of the back baffle and the back of the object is smaller, allowing for the less severe recirculation behind (downstream of) the object in Figure 16.

Validation of these computations is shown in Figure 18, the smoke test results for this configuration. The smoke test shows loss of containment, vortices behind (downstream of) the sash and person, and recirculation behind (downstream of) the object. Differences between the computation and the smoke test results are, as before, the size of the vortex behind (downstream of) the sash and, to a lesser extent, the flow behind (downstream of) the object. The computation does a better job of predicting the flow pattern over the top of the object but does not exactly match the gentler angle of flow coming off the back baffle towards the object.

Figure 19 displays the results of the contamination computation. As seen in Figure 19, the contaminant follows the airflow patterns shown in Figure 15. A small concentration of contaminant moves from the top of the object, down the front face of the object, and out of the fume hood main chamber. As predicted by the airflow structure, the fume hood loses containment of the contaminant.

Another configuration was studied at the 30.25 in. (0.77 m) sash height with the object moved back to 9 in. (0.23 m) behind

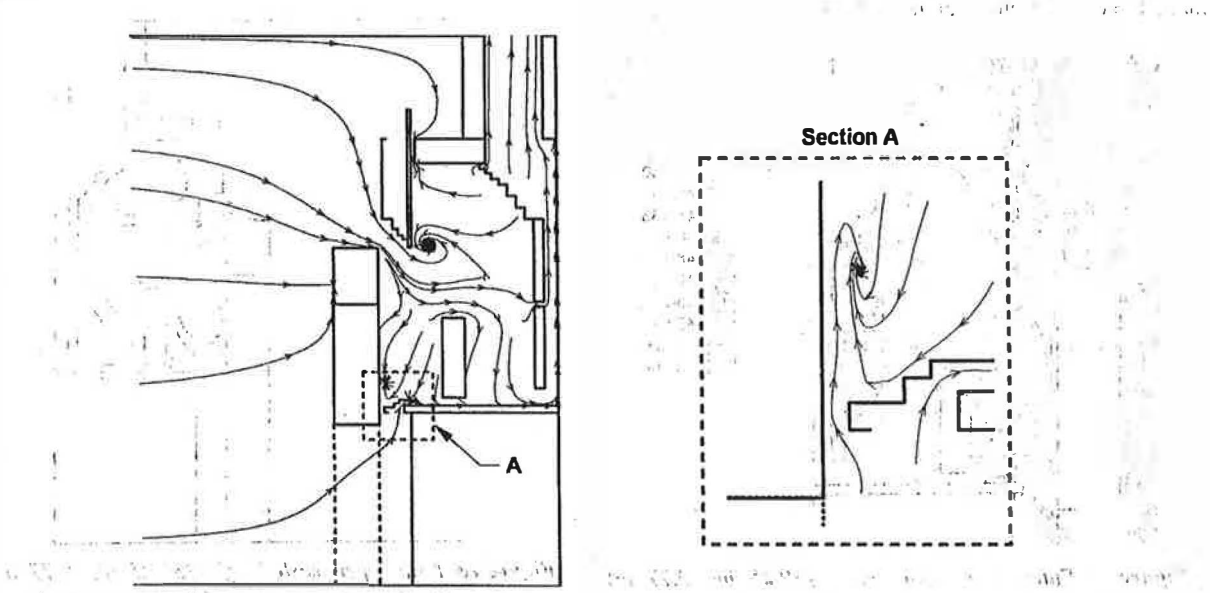

Figure 15 *Fully open sash height (30.25 in., 0.77 m), vertical slice, person, object at 6 in. (0.15 m), computational results.*

BACK TO PAGE ONE

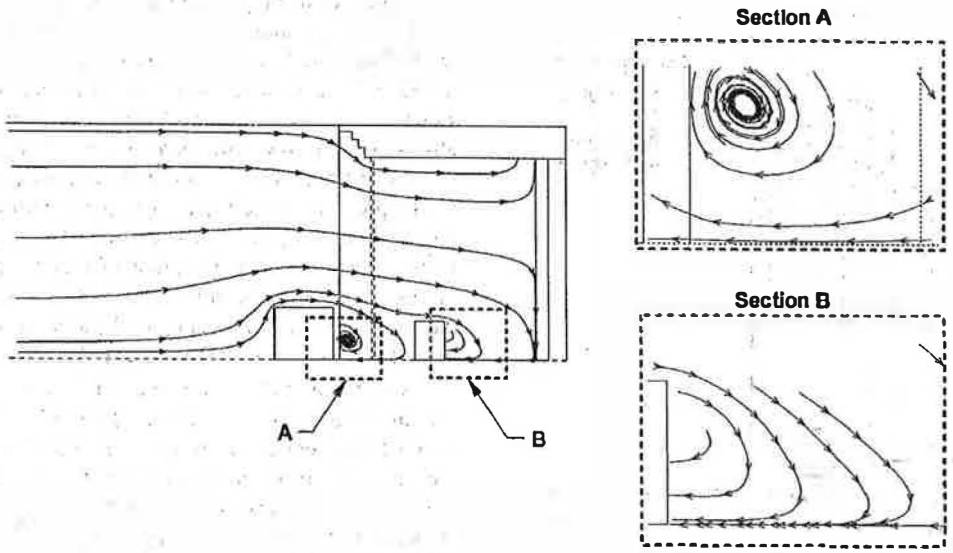

Figure 16 *Fully open sash height (30.25 in., 0.77 m), horizontal slice, person, object at 6 in. (0.15 m), computational results.*

the sash. The objective was to see whether containment could be maintained by the fume hood with the object moved farther away from the opening. The computed results are shown in Figure 20, and smoke test results are shown in Figure 21. The computed flow patterns agree very well with the smoke traces. The model again predicts the containment will be lost, which is confirmed by the smoke tests. In this configuration, the model does better at predicting the flow behind (downstream of) the object, giving it a more angled slope from the back baffle towards the object. In addition, two small vortices were predicted at the end of the bottom airfoil and at the top of the main fume hood chamber near the sash. These were not confirmed by the smoke tests. No horizontal slice is presented here, since it is very similar to the previous horizontal slice at the same sash height and lower sash velocity.

CONCLUSIONS

It has been shown that a three-dimensional CFD analysis can provide a simulation of laboratory fume hood airflow given appropriate boundary conditions. The three-dimensional fume hood model includes: airfoils, angled slotted baffles, a variable height sash, top and bottom bypasses, a

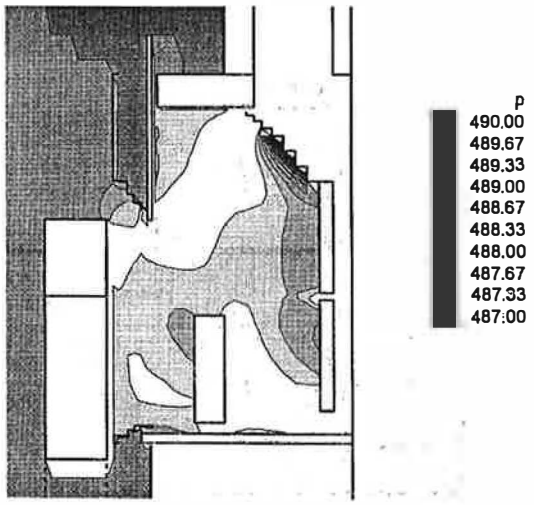

Figure 17 *Fully open sash height (30.25 in., 0.77 m), vertical slice, person, object at 6 in. (0.15 m), nondimensional pressure contour.*

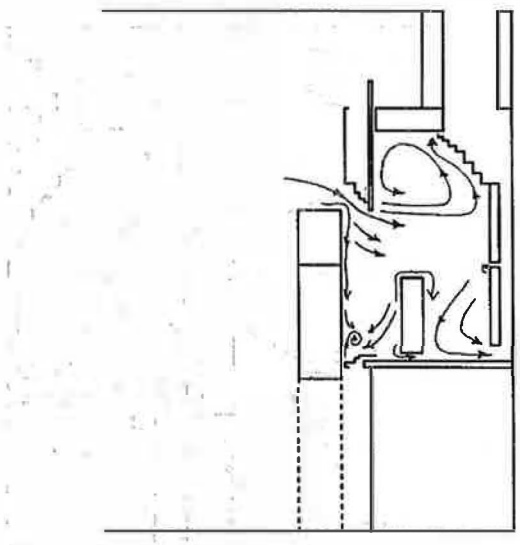

Figure 18 *Fully open sash height (30.25 in., 0.77 m), vertical slice, person, object at 6 in. (0.15 m), smoke test results.*

BACK TO PAGE ONE

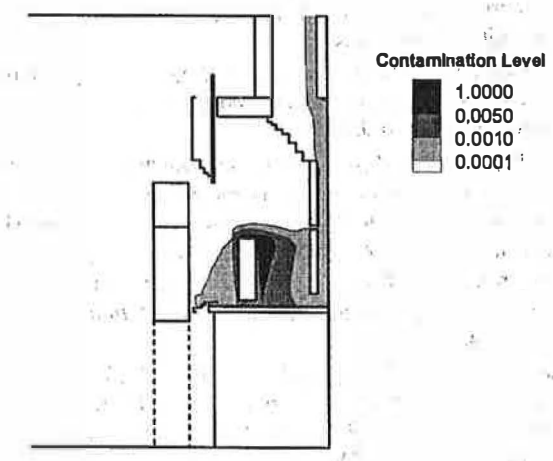

Figure 19 Fully open sash height (30.25 in., 0.77 m), vertical slice, person, object at 6 in. (0.15 m), nondimensional contamination results.

person, and an object. The results indicate that the room outside the fume hood is an essential component of the fume hood model to predict the expected flow patterns (large vortex behind the sash). The addition of the room to the fume hood simulation adds complexity and computation time but also allows investigation of external influences to fume hood airflow.

The three-dimensional simulation results produced flow patterns confirmed by smoke tests. The model is able to reproduce the large vortex behind (downstream of) the sash at different sash heights, as well as the small vortex created by a person in front of a fume hood and the recirculation behind (downstream of) an object in the fume hood. Also predicted by the simulation and confirmed by the smoke tests is the loss of

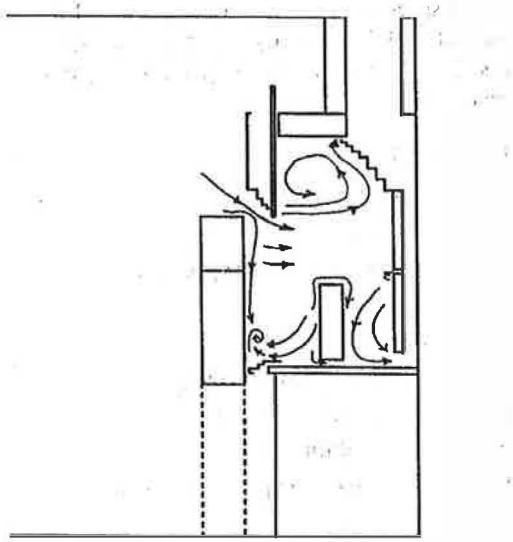

Figure 21 Fully open sash height (30.25 in., 0.77 m), vertical slice, person, object at 9 in. (0.23 m), smoke test results.

containment at the fully open sash height with a person and object added to the model. This flow pattern was repeated when the object was moved farther away from the sash, which did not improve containment problem. The model and smoke tests revealed containment was regained when the sash height was reduced.

ACKNOWLEDGMENTS

ASHRAE provided funding for the entire study under ASHRAE RP-848, *A Mathematical Model for the Prediction of Laboratory Fume Hood Airflow.* The work would not have been possible without the support of ASHRAE.

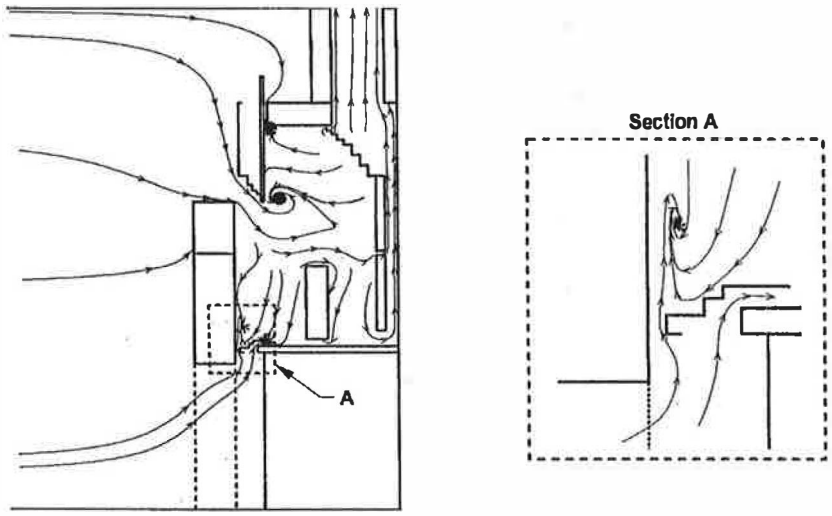

Figure 20 Fully open sash height (30.25 in., 0.77 m), vertical slice, person, object at 9 in. (0.23 m), computational results.

BACK TO PAGE ONE

A special thanks to Steve Eberhart and Julie Laufmann of the National Seed Storage Laboratory for providing the fume hood and laboratory space to perform the experimental investigations.

NOMENCLATURE

u_j = x, y, or z velocity
t = time
x_j = x, y, or z coordinate direction
p = pressure
ρ = density
k = turbulent kinetic energy
ν = kinematic viscosity
ν_t = eddy diffusivity
β = volumetric expansion coefficient
g = gravity
θ = temperature
ε = dissipation rate of turbulent energy
c = instantaneous concentration for passive contaminant
D = molecular diffusion coefficient for passive contaminant
s = volume contaminant generation source

REFERENCES

ASHRAE. 1995. *ANSI/ASHRAE Standard 110, Method of test performance of laboratory fume hoods.* Atlanta: American Society of Heating, Refrigerating and Air-Conditioning Engineers, Inc.

Chang, S.K.W. 1994. Air velocity profiles around a person standing in front of exhaust hoods. *ASHRAE Transactions* 100(2): 439-447.

Durst, F., and J.C.F. Pereira. 1991. Experimental and numerical investigations of the performance of fume cupboards. *Building and Environment*, Vol. 26(2): 153-164.

Knapmiller, K., and A. Kirkpatrick. 1994. Computational determination of the behavior of a cold air ceiling jet in a room with a plume. *ASHRAE Transactions* 100(1): 677-684.

Kurabuchi, T., J.B. Fang, and R.A. Grot. 1989. *A numerical method for calculation indoor airflows using a turbulence model, NISTIR 89-4211.* Gaithersburg, Md.: National Institute of Standards and Technology.

Launder, B.E., and D.B. Spalding. 1974. The numerical computation of turbulent flows. *Computer Methods in Applied Mechanics and Engineering* Vol. 3: 269-289.

Neilsen, P.V. 1998. The selection of turbulence models for the prediction of room airflow. *ASHRAE Transactions* 104(1).

Pathanjali, C., and M.M. Rahman. 1996. Study of flow patterns in fume hood enclosures. Proceedings of the 31st Intersociety Energy Conversion Engineering Conference, IECEC, August 11-16, Washington, D.C. Vol. 3: 2003-2008.

Sanders, G.T. 1993. *Laboratory fume hoods: A user's manual*, Chapter 3, pp. 18-21. Jon Wiley & Sons Inc.